Journal of Applied Electrochemistry **32**: 1341–1346, 2002.

Electrochemical study of the chromium electrode behaviour in borate buffer solution

D. MARIJAN[1,*] and M. GOJIĆ[2]
[1]*Pliva, Pharmaceutical Industry, Incorporated, Research & Development, Prilaz baruna Filipovića 25, 10000 Zagreb, Croatia;*
[2]*Faculty of Metallurgy, University of Zagreb, Aleja narodnih heroja 3, 44103 Sisak, Croatia;*
*(*author for correspondence)*

Received 24 July 2001; accepted in revised form 30 July 2002

Key words: capacitor, chromium electrode, chromium passivity, transpassive dissolution

Abstract

The electrochemical behaviour of the chromium electrode in borate buffer solution (pH 9.3) was studied by cyclic voltammetry and electrochemical impedance spectroscopy. Chromium passivity was observed over a broad potential region, from −1.0 to 0.5 V vs SCE. The passivation process took place in two steps: formation of a chromium oxide monolayer and transition of chromium to a higher valence state. The anodic film exhibited the properties of a p-type semiconductor. Transpassive dissolution of chromium occurred at 0.5 V vs SCE, with two reaction intermediates present, Cr^{III}_{Cr} and Cr^{4+}_{ad}.

1. Introduction

The corrosion and passivation behaviour of iron, nickel and chromium is one of the most investigated problems in electrochemical science and technology [1–3]. This is due to the central role these metals play as basic materials in many industries (metallurgical, chemical and pharmaceutical). There is a great economic incentive to develop methods and materials to alleviate corrosion; this can be achieved only by a detailed understanding of the mechanisms and processes involved in this complex phenomenon.

Interest in chromium passivity dates back to the end of the nineteenth century [4]. Since then, chromium has positioned itself as one of the most beneficial alloying agents for corrosion-resistant engineering alloys, such as stainless steels [5, 6] or nickel-based alloys [7]. The results of passivity tests of stainless steels and nickel-based alloys can be explained on the basis of the electrochemical behaviour of pure metals.

The chemical composition and physical properties of passive films on chromium metal are still a matter of debate [8–13]. Early X-ray photoelectron spectroscopy (XPS) spectra [8] of a passive film that formed on chromium in sulphuric acid were attributed to a hydrated form of Cr_2O_3. Based on ellipsometric and Auger analyses, Seo et al. [9] concluded that the passive film on chromium had a stoichiometry almost equal to that of Cr_2O_3. He also believed that the outer surface layer was most probably hydrated. Likewise, Haupt and Strehblow [10] interpreted their XPS results for the passive film on chromium as a Cr_2O_3 matrix containing some water. On the other hand, Heumann and Panesar [11] excluded the presence of Cr_2O_3 and suggested that the passive layer consisted of CrOOH. On the basis of XPS analysis [12], the formation of a mixed Cr(III), Cr(II) oxy-hydroxide having the general formula $2\alpha CrO_{1.5-m}(OH)_{2m}(1-2\alpha)CrO_2$ (with $0 \leqslant m \leqslant 1.5$ and $0 \leqslant \alpha \leqslant 0.5$) has been proposed.

Bojinov et al. [13] studied the passive state of chromium in 1 M sulfate solution by applying a combination of electrochemical techniques. They suggest that the passive film growth was associated with an exponential increase in the film resistance, probably as a result of simultaneous dehydration/oxidation of Cr(II) to Cr(III) through a solid-state electrochemical reaction. It can be assumed that the film in the potential region essentially consisted of Cr_2O_3.

Many electrochemical and surface analytical techniques have been used in studies of the corrosion behaviour of pure metals and iron–chromium alloys [14, 15]. Cyclic voltammetry and electrochemical impedance spectroscopy (EIS) provide a good insight into the chemical processes that occur during passivation [16, 17]. By means of the impedance measurements more information about a system can be obtained from a single experiment than by other electrochemical methods. However, the impedance spectra contain the information in an implicit form. A careful multistep analysis is needed to allow it to be understood in physicochemical terms. The key steps of analysis are measurement modelling and process modelling [17].

Despite many investigations [18–22], the nature of the passive film on chromium is still poorly understood. The

aim of this work was to investigate the anodic behaviour of chromium in the potential range from the hydrogen evolution reaction to transpassive dissolution of chromium metal in borate buffer solution by means of cyclic voltammetry and electrochemical impedance spectroscopy.

2. Experimental details

Electrochemical experiments were performed in a deaerated borate buffer solution consisting of 0.022 M $Na_2B_4O_7 \cdot 10\ H_2O$ and 0.002 M NaOH (pH 9.3) using an EG&G PAR model 273 potentiostat/galvanostat, with a model 5301 lock-in amplifier. The electrolyte was prepared with distilled water and analytical grade sodium borate and sodium hydroxide (*pro analysi*). All electrochemical measurements were carried out at room temperature and at a selected electrode rotation rate of 1600 rpm.

A conventional three-compartment glass cell was used. A platinum grid of large area served as counter electrode. The reference electrode was the saturated calomel electrode (SCE). All potentials are referred to the SCE scale. The working electrode was a 99.996% pure chromium rod embedded in a PTFE holder, with an exposed area of 0.196 cm^2. A rotating disc electrode (RDE) was used. The RDE was polished with silicon carbide paper. For finish a 1000 grade paper was used. The electrode was rinsed with distilled water and cleaned ultrasonically in ethanol. It was then again rinsed in distilled water and dried in air.

Before polarization measurements, the working electrode was polarized at −1.2 V in borate buffer solution for 300 s to provide a reproducible electrode surface [23]. Further pretreatment yielded equal results.

Impedance measurements were performed in the potential range from −1.2 to 0.8 V. Before measurement, the working electrode was first polarized at −1.2 V in borate buffer solution for 300 s and then potentiodynamically at a scan rate of 10 mV s^{-1} with respect to previously chosen constant potentials. The electrode stabilization time at constant potential was 120 s before measurement. Impedance measurements were carried out in the frequency range 50 kHz–40 mHz at eight points $(decade)^{-1}$ with a sinusoidal amplitude of 5 mV.

3. Results

Figure 1 shows the cyclic voltammogram of chromium in borate buffer solution. A sharp active–passive transition was not observed as in acidic solutions [18]. A wide plateau of the potential-independent current indicates that chromium passivity was present over a broad potential region (from −1.0 to 0.5 V). The transpassive reaction became apparent as the potential was increased beyond 0.5 V. According to the Pourbaix [24] diagram, chromate ions (CrO_4^{2-}) are produced in that potential

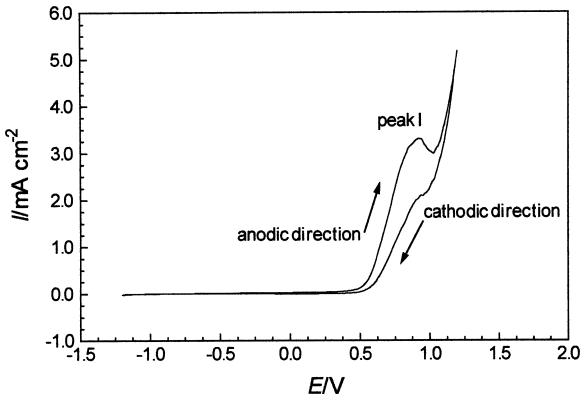

Fig. 1. Cyclic voltammogram of chromium in borate buffer solution in the potential range from −1.2 to 1.2 V. Scan rate 10 mV s^{-1}. *E* – potential; *I* – current density.

region. The peak I (about 0.85 V) in the cyclic voltammogram (Figure 1) marks the beginning of secondary passivity. The appearance of secondary passivity was due to the onset of the formation of CrO_4^{2-} and oxygen evolution.

Figure 2 shows the cyclic voltammogram from Figure 1, but in a narrower potential range (from −1.0 to 0.5 V). The current slowly increases in the anodic direction in the passive range. The peak II in Figure 2 marks the onset of chromium oxide reduction i.e. of the process of transformation of Cr(VI) to Cr(III) [25].

Figures 3–6 show impedance diagrams obtained at various selected potentials. The chosen diagrams clearly portray a change in impedance with change in potential. Both Nyquist and Bode diagrams are displayed. A number of equivalent circuits were applied for analysis of experimental impedance data, including the Randles model with one time constant. The nonlinear least-squares computer program developed by Boukamp [26] was used for impedance analysis. The relative residual errors defined as a span between the experimental and calculated data were used to determine a χ^2-function, which helped evaluate whether the equivalent circuit model and parameter set adequately described the

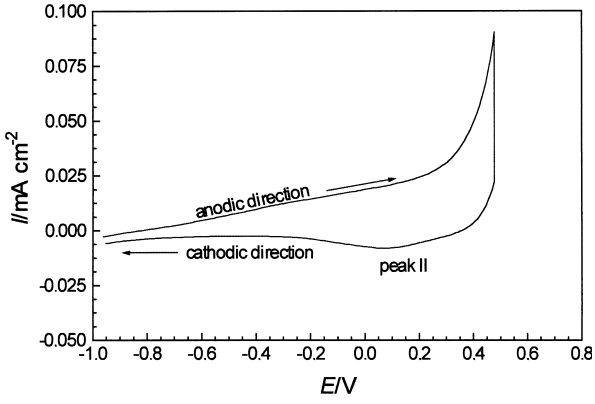

Fig. 2. Cyclic voltammogram of chromium in borate buffer solution in the potential range from −1.2 to 0.5 V. Scan rate 10 mV s^{-1}. *E* – potential; *I* – current density.

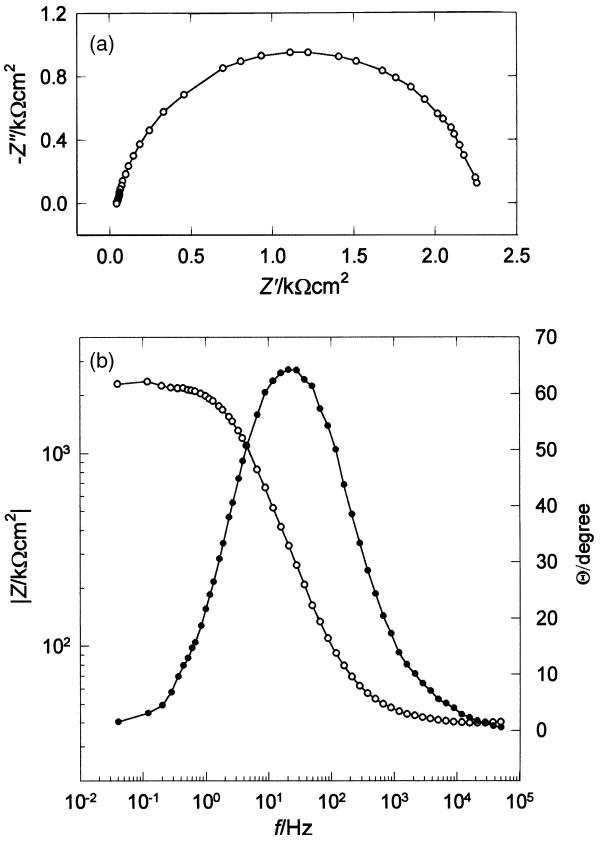

Fig. 3. Nyquist (a) and Bode (b) impedance diagrams of chromium at −1.2 V in borate buffer solution. Z' – real impedance; Z'' – imaginary impedance; $|Z|$ – absolute impedance (°); θ – phase angle (•); f – frequency.

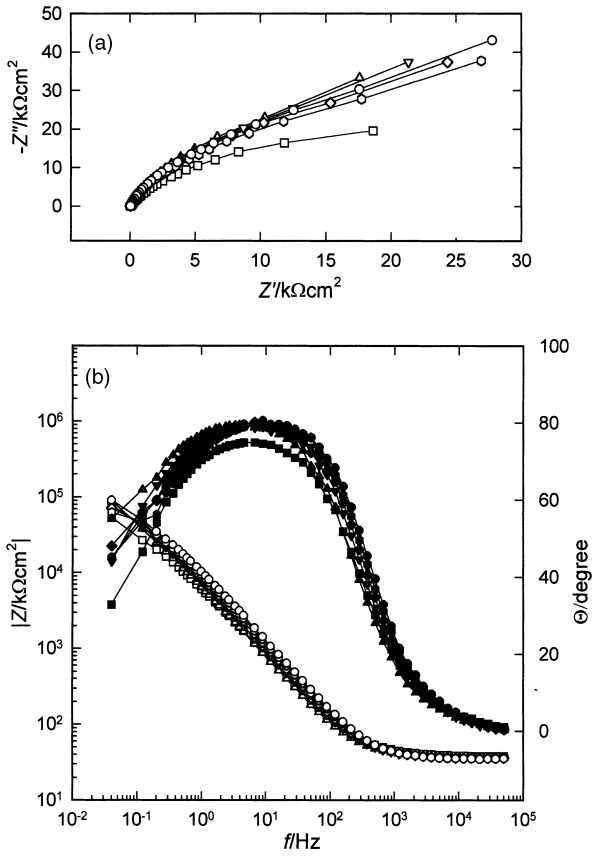

Fig. 4. Nyquist (a) and Bode (b) impedance diagrams of chromium in the passive range in borate buffer solution. Symbols as for Figure 3. Key: (□) −1.0, (△) −0.8, (▽) −0.6, (◇) −0.3, (⬡) 0 and (○) +0.3 V.

measured data. Application of the model having two time constants yielded lower values of the χ^2-function depicting the practicability of the model.

Figure 7 shows equivalent circuits adapted for analysis of experimental impedance data within the limits of experimental error ($\chi^2 = 10^{-4}$) and of data reproducibility. R_{el} is the ohmic resistance or uncompensated resistance of the solution between chromium and the referent SCE electrode. Q is the constant phase element (CPE) and W is the Warburg impedance. A dispersive behaviour observed at the chromium electrode surface was described by means of CPE, which was defined in the impedance form as [27]:

$$Z_{CPE} = [Q(j\omega)^n]^{-1} \quad (1)$$

where n is associated with the roughness of the electrode surface and has a value between 0.5 (porous electrode) and unity (ideally flat electrode), j is $\sqrt{-1}$, and ω is angular frequency ($\omega = 2\pi f$, where f is frequency). Impedance measurements were interpreted in terms of charge transfer resistance R_{ct} [28].

$$R_{ct} = \lim_{\omega \to 0} R(Z_f) \quad (2)$$

where $R(Z_f)$ denotes the real part of the complex faradaic impedance Z_f and ω corresponds to the frequency of the a.c. signal.

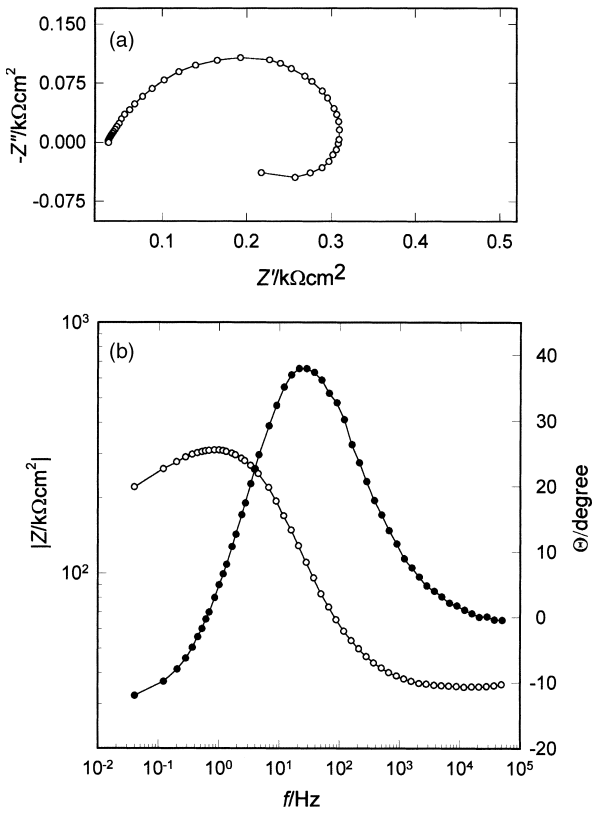

Fig. 5. Nyquist (a) and Bode (b) impedance diagrams of chromium at 0.6 V in borate buffer solution. Symbols as for Figure 3.

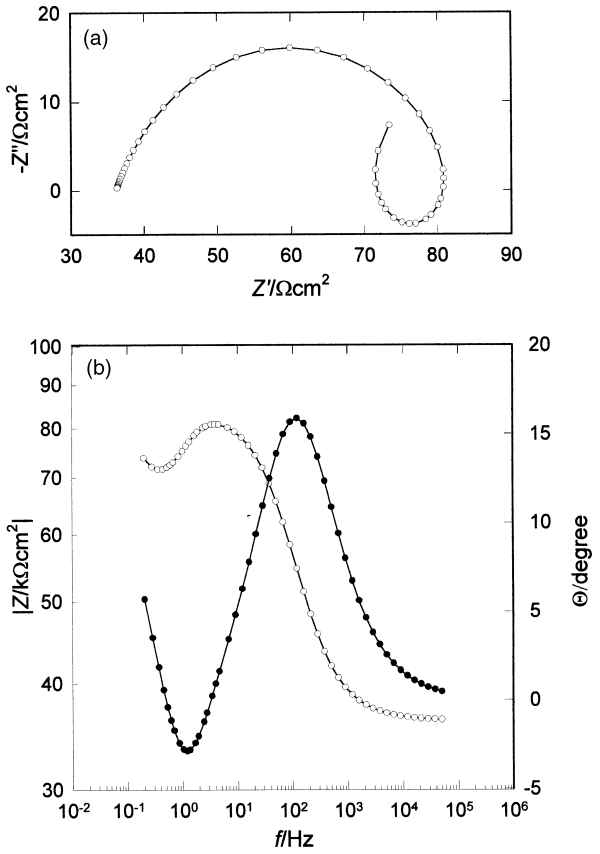

Fig. 6. Nyquist (a) and Bode (b) impedance diagrams of chromium at 0.8 V in borate buffer solution. Symbols as for Figure 3.

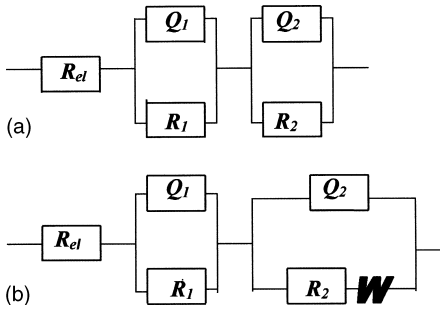

Fig. 7. Equivalent circuits of impedance measurement for chromium in different potential ranges: (a) hydrogen evolution reaction; (b) passive region. R_{el} – ohmic resistance; Q – constant phase element; R – resistance; W – Warburg impedance.

The impedance plot (Figure 3(a)) measured at −1.2 V showed a capacitive loop with a relatively small R_{ct} value (2.2 kΩ cm^2). The data were fitted to an equivalent circuit consisting of (R_1Q_1) and (R_2Q_2) series combinations (Figure 7(a)). This equivalent circuit adequately described the measured data, whereas the equivalent circuit with one time constant did not ($\chi^2 = 10^{-3}$). In the former case lower values of the χ^2-function were obtained ($\chi^2 = 10^{-4}$).

This behaviour has been attributed to the hydrogen evolution reaction taking place at the chromium passive surface [29]. By increasing the potential polarization from −1.0 to 0.3 V, the R_{ct} values increased and the equivalent circuits consisting of R_{el} and (R_1Q_1) and $Q_2(R_2W)$ series combination were used to fit the experimental data (Figure 7(b)). An apparent Warburg impedance in the passive range indicated a contribution of a diffusion process [30]. Transpassive dissolution of chromium began at a potential above 0.4 V. Figure 5 shows an impedance spectrum in the transpassive range of chromium at 0.6 V. Capacitive and inductive loops nevertheless appeared. With increase in potential up to 0.8 V, both capacitive and inductive loops were well defined (Figure 6).

4. Discussion

The absence of the activation maximum on the I/E curve in Figure 1 can be explained by the fact that even a brief contact of chromium with moist air was sufficient to create a thin oxide layer on the electrode surface, which then prevented further active chromium dissolution. The increase in passive current with increasing potential (Figure 2) can be interpreted in terms of the point defect model developed by Macdonald [31].

The increase in potential polarization in the anodic direction favours the production of metal vacancies near the film–solution interface [32]. Thus, the passive current is predicted to increase with increasing potential, as found experimentally (Figure 2). Since the Q value is identical to capacity at $\omega = 1$, the capacity of the space charge layer (C) is determined by means of the following equation:

$$\frac{1}{C} = \frac{1}{Q_1} + \frac{1}{Q_2} \tag{3}$$

From the slope in Figure 8, which shows capacitance versus potential in Mott–Schottky coordinates, it can be concluded that the anodic film formed on chromium can be regarded as a p-type semiconductor and the acceptor-

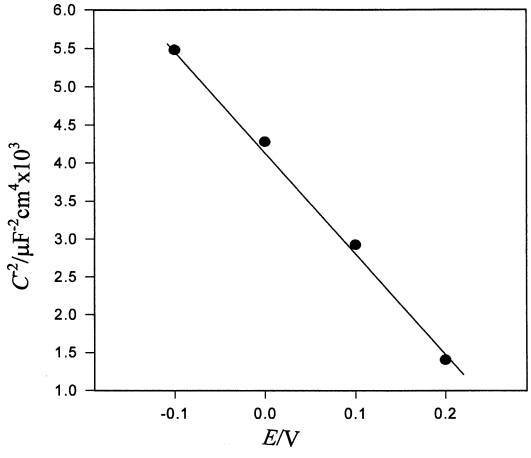

Fig. 8. Relationship between capacitance and potential polarization in the polarization range from −0.1 to 0.2 V for chromium in the Mott–Schottky coordinates.

type conductivity is valid for the potential range from −0.2 to 0.2 V.

According to the Nyquist diagram for chromium (Figure 3(a)), a capacitive loop was obtained at −1.2 V (in the hydrogen evolution reaction region) with the R_{ct} value of 2.2 kΩ cm^2. Increase in the potential from −1.2 to 0.6 V produced different R_{ct} values (Figure 9). In the potential range from −1.2 to −0.4 V, R_{ct} increased with increasing potential. A number of processes are possible candidates to explain this phenomenon. Film growth can occur as a result of the rising potential [33], and the composition of the passive film tends to change with potential [34]. The presence of the Warburg impedance (Figure 7(b)) for the potential range from −1.0 to 0.2 V points to a diffusion process taking place on/through the passive film. At potentials above −0.4 V, the R_{ct} values decreased with increasing potential. This was likely due to the formation and presence of Cr(VI) species in the passive film before transpassive dissolution of chromium. A more fundamental description in terms of a transfer function will be needed in further investigation.

Passivation of pure chromium was carried out in two steps. The first step is assumed to have been due to the formation of a (monolayer) chromium oxide passive film, while in the second step there was a transition of chromium to a higher valence state. Thus, the passivation behaviour of chromium (the passivation reaction is proposed to be the oxidation of divalent adsorbed hydroxide to trivalent oxide–hydroxide [18]) is given by:

$$Cr + H_2O \rightarrow CrOH_{ad} + H^+ + e^- \quad (4)$$

$$CrOH_{ad} + H_2O \rightarrow Cr(OH)_{2,ad} + H^+ + e^- \quad (5)$$

$$Cr(OH)_{2,ad} \rightarrow CrOOH_{ad} + H^+ + e^- \quad (6)$$

The transpassive region of chromium begins at about 0.5 V as indicated by a faster increase of the current (Figures 1 and 2). Nyquist plots of electrochemical impedance responses corresponding to transpassive dissolution of chromium in borate buffer solutions show capacitive and inductive behaviour above 0.5 V (Figures 5(a) and 6(a)). The appearance of an inductive loop semicircle at 0.6 and 0.8 V indicate a reaction intermediate (Figures 5(a) and 6(a)). These results agree qualitatively with the results of Bojinov et al. [35], which were obtained in an identical solution, but at low rotation rates (below 300 rpm). Bojinov claimed that there were two reaction intermediates during chromium transpassive dissolution. The processes occurring in the chromium/anodic passive film/solution system during dissolution are as follows:
at a chromium/film interface:

$$V_{Cr}^{3-} + Cr_m \rightarrow Cr_{Cr}^{III} + V_m + 3\,e^- \quad (7)$$

at a film/solution interface

$$Cr_{Cr}^{III} \rightarrow Cr_{ad}^{4+} + V_{Cr}^{3-} + e^- \quad (8)$$

at a film/solution interface

$$Cr_{ad}^{4+} + 4\,H_2O \rightarrow CrO_4^{2-} + 8\,H^+ + 2\,e^- \quad (9)$$

The total reaction concerning the mechanism of transpassive chromium dissolution as proposed by El-Basiony et al. [36] is

$$2\,Cr + 7\,H_2O \rightarrow Cr_2O_7^{2-} + 14\,H^+ + 12\,e^- \quad (10)$$

and that proposed by Sato [37] is:

$$Cr_2O_3 + 5\,H_2O \rightarrow 2\,CrO_4^{2-} + 10\,H^+ + 6\,e^- \quad (11)$$

At pH 9.3 and assuming the $Cr_2O_7^{2-}$ and CrO_4^{2-} activities to be 1, the chromate ion is more dominant in the Pourbaix diagram than the dichromate ion. This is in accordance with the results of Kelsall et al. [38] based on the potential–pH diagrams for the Cr/H_2O system at 25 °C. $Cr_2O_7^{2-}$ ions are formed at pH < 6 and CrO_4^{2-} ions at pH > 6. The CrO_4^{2-} ions are known for their corrosion inhibiting effect [39, 40].

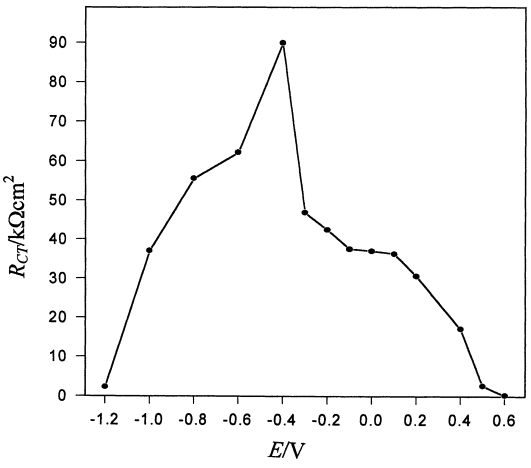

Fig. 9. Relationship between R_{ct} and potential polarization for chromium in borate buffer solution (pH 9.3).

5. Conclusion

Passivation of the chromium electrode occurred in two steps: formation of a chromium oxide monolayer and transition of chromium to a higher valence state. Increase in the potential from −1.2 to 0.6 V produced an effect on the value of charge transfer resistance (R_{ct}). In the range −1.2 to −0.4 V, R_{ct} increased with increasing potential, while above −0.4 V, R_{ct} decreased with increasing potential. Numerous processes that may explain these phenomena have been discussed. However, a more fundamental description in terms of transfer function will be needed in further investigation.

References

1. L.J. Oblonsky and T.M. Devine, *Corros. Sci.* **37** (1995) 17.
2. P. Schmuki, S. Virtanen, A.J. Davenport and C.M. Vitus, *J. Electrochem. Soc.* **143** (1996) 3997.
3. A.J. Devenport, L.J. Oblansky, M.P. Ryan and M.F. Toney, *J. Electrochem. Soc.* **147** (2000) 2162.
4. T.P. Moffat and R.M. Latanision, *J. Electrochem. Soc.* **139** (1992) 1869.
5. M.G.S. Ferreira, T. Moura de Silva, A. Catarino, M. Pankuch and C.A. Melendres, *J. Electrochem. Soc.* **139** (1992) 3146.
6. M. Gojić, D. Marijan and L. Kosec, *Corrosion* **56** (2000) 839.
7. D. Marijan, M. Vuković, P. Pervan and M. Milun, *J. Appl. Electrochem.* **28** (1998) 96.
8. G. Bouyssoux, M. Romand, H.D. Polaschegg and J.T. Calow, *J. Electron Spectrosc.* **11** (1977) 185.
9. M. Seo, R. Saito and N. Sato, *J. Electrochem. Soc.* **127** (1980) 1909.
10. S. Haupt and H.H. Strehblow, *J. Electroanal. Chem.* **228** (1987) 365.
11. T. Heumann and H.S. Panesar, *J. Electrochem. Soc.* **110** (1963) 628.
12. M.N. Shlepakov, A.M. Sukhotin, Y.P. Kostikov and E.G. Kuz'mina, *Elektrohimiya* **22** (1986) 125.
13. M. Bojinov, G. Fabricius, T. Laitinen, T. Saario and G. Sundholm, *Electrochim. Acta* **44** (1998) 247.
14. S. Haupt and H.H. Strehblow, *Corros. Sci.* **37** (1995) 43.
15. C-O.A. Olsson, D. Hamm and L. Landolt, *J. Electrochem. Soc.* **147** (2000) 4093.
16. M. Itagaki, A. Matsuzaki and K. Watanabe, *Corros. Sci.* **37** (1995) 1867.
17. P. Zoltowski, *J. Electroanal. Chem.* **375** (1994) 45.
18. L. Björnkvist and I. Olefjord, *Corros. Sci.* **32** (1991) 231.
19. B. Stypula and J. Banas, *Electrochim. Acta* **38** (1993) 2309.
20. T. Hurlen, S. Hornkjol and E. Gulbrandsen, *Electrochim. Acta* **38** (1993) 643.
21. C.A. Acosta, R.C. Salvarezza, H.A. Widela and A.J. Arvia, *Corros. Sci.* **25** (1985) 291.
22. M. Bojinov, G. Fabricius, T. Laitinen, K. Makela, T. Saario and G. Sundholm, *Electrochim. Acta* **45** (2000) 2029.
23. E.B. Castro, J.R. Wilche and A.J. Arvia, *Corros. Sci.* **32** (1991) 37.
24. M. Pourbaix, 'Atlas of Electrochemical Equilibria in Aqueous Solutions', 2nd edn (NACE, Houston, TX, 1974).
25. B. Baverskog and I. Puigdomenech, *Corros. Sci.* **39** (1997) 43.
26. B.A. Boukamp, *Solid State Ionics* **20** (1986) 31.
27. U. Rammelt and G. Reinhard, *Electrochim. Acta* **35** (1990) 1045.
28. I. Epelboin, K. Kedam and H. Takenouti, *J. Appl. Electrochemistry* **2** (1972) 71.
29. B.E. Wilde and B.F. Hodge, *Electrochim. Acta* **14** (1969) 619.
30. S.R. Taylor and E. Gileadi, *Corrosion* **51** (1995) 664.
31. D.D. Macdonald, *J. Electrochem. Soc.* **139** (1992) 3434.
32. M. Bojinov, G. Fabricius, T. Laitinen, K. Mäkelä and T. Saario, *Electrochim. Acta* **45** (2000) 2029.
33. N. Seo and N. Sato, Proc. 12th International Corrosion Congres, Houston, TX, 19–24 Sept. 1993; NACE International, 3B (1993), p. 171.
34. N. Hara and K. Sugimoto, *J. Electrochem. Soc.* **126** (1979) 1328.
35. M. Bojinov, G. Fabricius, T. Laitinen and T. Saario, *in* 'Proceedings of EUROCORR '99', The European Corrosion Congress, Vol. 2, Trondheim (1997), p. 622.
36. M.S. El-Basiouny and S. Haruyama, *Corros. Sci.* **17** (1972) 121.
37. N. Sato, *Corros. Sci.* **31** (1990) 1.
38. G.H. Kelsall, C.I. House and F.P. Guyanga, *J. Electroanal. Chem.* **244** (1988) 179.
39. C.R. Clayton and Y.C. Lu, *Corros. Sci.* **29** (1989) 881.
40. Y.C. Lu, C.R. Clayton and A.R. Brooks, *Corros. Sci.* **29** (1989) 863.